Research Article

Experimental Study and Analysis of Sulfur Dioxide Recovery Efficiency from the Exhaust Gases of a Sulfur Production Unit

Akbar Darvishi

Department of Chemical Engineering, Fir.C., Islamic Azad University, Firoozabad, Iran

ABSTRACT

In this study, the operational conditions affecting sulfur dioxide recovery in a single-phase fluidized bed reactor using aluminum oxide as a catalyst were investigated. The research includes both experimental and theoretical analyses of reactor performance, with the main goal of producing a sweet gas stream. A series of experiments were conducted using sour gas streams containing different concentrations of sulfur dioxide. The effects of key parameters—including bed height, bed width, alumina particle diameter, and operational conditions such as temperature, pressure, and gas superficial velocity—were systematically evaluated and discussed. A comparative analysis was made between the experimental data for bed height, temperature, and alumina content and the corresponding model predictions. The findings reveal minor discrepancies between the experimental and theoretical results. The results indicate a positive correlation between sulfur dioxide recovery and both alumina content and bed height. Moreover, a relatively linear relationship was observed between sulfur dioxide recovery and operating temperature. This study provides valuable insights into the influence of operating parameters on sulfur dioxide recovery in a fluidized bed reactor using aluminum oxide as an adsorbent.

ARTICLE INFO

Introduction

Sulfur occurs in nature both in elemental form and in combination with minerals and hydrocarbons [1]. The global amount of sulfur is significant, estimated at around 3,500 million tons, of which at least 40% can be economically recovered [2]. Major sulfur deposits are distributed as follows: 18% in Russia and Central Asia, 11% in Canada, and 10% in the United States [3]. Elemental sulfur can remain trapped underground or be extracted using the *Frasch process*, in which hot water is pumped through concentric pipes into sulfur-containing layers to melt the sulfur and bring it to the surface for recovery [4]. This recovered sulfur,

with high commercial purity, can be marketed either in pure form or combined with mineral sulfur [5].

The development of the liquid absorption–oxidation processes marked the beginning of industrial sulfur recovery, which later reached a major milestone with the invention of the Claus process (direct oxidation) [6]. Over the past century, all processes handling acid gas streams with high hydrogen sulfide concentrations (greater than 10%) have utilized the Claus process. Although numerous modifications have been made, the fundamental principle of the process has remained unchanged [7].

Today, besides the Claus process—which is primarily used for the removal of high H_2S concentrations—biological methods and direct sulfur production from H_2S are also applied, especially for lower concentrations, either simultaneously or sequentially with gas sweetening processes. The sulfur present in hydrocarbons, mostly in the form of hydrogen sulfide, is recovered using various technologies [8]. Modern sulfur recovery processes can be classified into two main categories: liquid absorption–oxidation processes and direct oxidation processes. Different derivatives of the Claus process have been developed to handle a wide range of feed gas compositions. The primary basis for classification is the percentage of H_2S in the feed, which depends on the composition of gases from gas wells or associated petroleum gases [9].

In some cases, additional *acid gas enrichment* steps are employed to increase the H_2S concentration before feeding it into Claus units [10]. These processes are often integrated with gas sweetening systems, using specially formulated amines that selectively absorb CO_2 over H_2S [11]. One example is Fluor Corporation's technology, which allows selective CO_2 removal and acid gas enrichment up to 75% H_2S in the Claus unit feed [12].

A pilot-scale unit was constructed to validate the developed mathematical model. The experimental setup included two fluidized bed reactors for sulfur dioxide adsorption. Each

reactor was packed with a fixed bed of alumina catalyst measuring seven meters in width and two meters in height. A schematic representation of the setup is shown in Figure 1, and an image of the reactor in Figure 2.
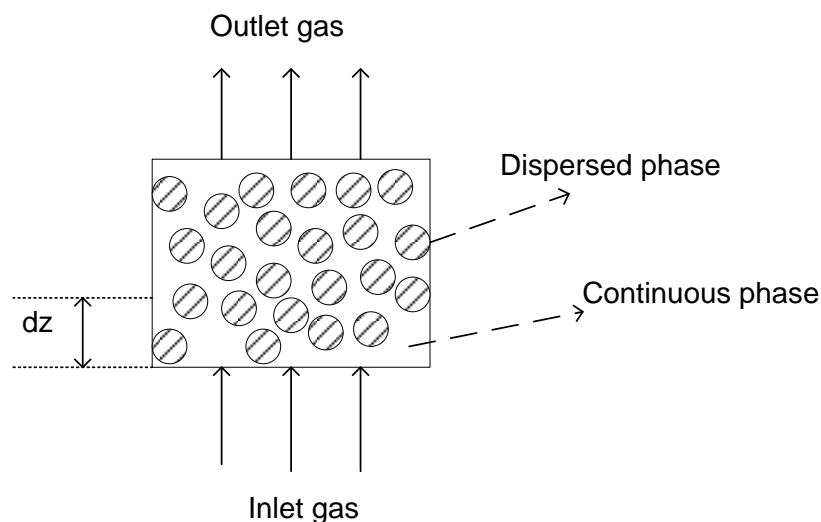

Fig.1. Schematic of a fluidized bed reactor.

Fig. 2. Image of a fluidized bed reactor.

Flue gas containing a defined concentration of SO_2 was introduced into the reactor. Inside the reactor, sulfur dioxide reacted with the catalytic bed, leading to a gradual decrease in SO_2 concentration along the bed height. The concentrations of sulfur dioxide in the inlet and outlet gas streams were determined using standard analytical techniques. Bed temperature, pressure, and gas flow velocity were measured during each experiment.

When the reactor's operating temperature was maintained between 700 °F and 800 °F, the catalysts achieved effective SO_2 removal from the gas stream. Hydrogen, methane, or carbon monoxide could be used as reducing agents for catalyst regeneration. The regeneration process, which removes adsorbed sulfur dioxide from the catalyst surface, typically occurs within a narrow temperature range—around 750–850 °F—close to that of the absorption stage.
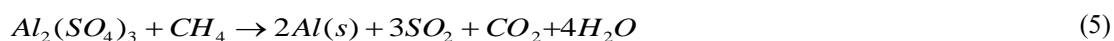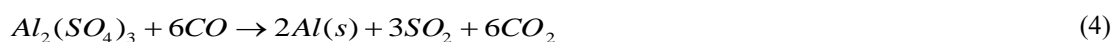
2. Experimental

2.2. Process Chemistry

The flue gas stream containing sulfur dioxide enters the reactor, which is packed with a bed of alumina catalyst. Inside the reactor, aluminum oxide reacts with the oxygen present in the gas stream to form aluminum sulfate. The reactions proceed according to Equations (1) and (2).

$$2Al_2O_3 + 6SO_2 + 3O_2 \rightarrow 2Al_2(SO_4)_3 \tag{1}$$
$$2Al_2O_3 + 3SO_2 \rightarrow Al_2(SO_4)_3 \tag{2}$$

The activation energy required for the reaction is 22.1 kJ mol⁻¹. During the regeneration process, aluminum sulfate is reduced to metallic aluminum while sulfur dioxide is released. A mixture of hydrogen and carbon monoxide—or alternatively light hydrocarbons—can be used as reducing agents in the regeneration process. Equations (3), (4), and (5) represent the reduction reactions occurring within the catalytic bed.

$$Al_2(SO_4)_3 + 6H_2 \rightarrow 2Al(s) + 3O_2 + 6H_2O \tag{3}$$
$$Al_2(SO_4)_3 + 6CO \rightarrow 2Al(s) + 3SO_2 + 6CO_2 \tag{4}$$
$$Al_2(SO_4)_3 + CH_4 \rightarrow 2Al(s) + 3SO_2 + CO_2 + 4H_2O \tag{5}$$

Furthermore, both alumina and aluminum sulfate exhibit selective catalytic activity toward the removal of nitrogen oxides (NO_x) within the fluidized bed reactor. Consequently, ammonia is injected into the flue gas stream before it enters the reactor. The injected ammonia reacts with the nitrogen oxide compounds in the presence of the catalyst within the bed, as described by Equations (6) and (7).

$$4NO + 4NH_3 + O_2 \rightarrow 4N_2 + 6H_2O \tag{6}$$

$$4NO_2 + 8NH_3 \rightarrow 7N_2 + 12H_2O \tag{7}$$

2.2. Mass Balance in the Dispersed Phase

The mass balance equations were derived based on the schematic representation shown in Figure 1. These equations incorporate two primary mechanisms of mass transfer:

1. Bulk mass transfer, resulting from the convective motion of the fluid, and

2. Molecular diffusion, driven by the concentration gradient of sulfur dioxide between the phases.

Equations (8) and (9) describe the mass balance within the dispersed phase. In this model, it is assumed that the solid catalyst particles are uniformly distributed throughout the dispersed phase, and that the sulfur dioxide concentration within this phase is a function of both time and position. The chemical reaction occurs at the interfacial surface between the gas phase and the catalyst particles; therefore, the overall mass-transfer rate is strongly influenced by the hydrodynamic conditions and the physical properties of the system.

$$\dot{m}_{bdis.} \mid_z - \dot{m}_{bdis.} \mid_{z+\Delta z} - \dot{m}_{mdis.} = m_{acc.} \tag{8}$$

$$A(U - U_{mf})C_d \mid_z - A(U - U_{mf})C_d \mid_{z+\Delta z} - N(Q + K_G A_b)(C_d - C_c) = V_d \frac{\partial C_d}{\partial t} \tag{9}$$

For the formulation of the mass balance in the dispersed phase, the gas flow is considered to be in a steady-state regime with negligible changes in gas density. Consequently, Equations (8) and (9) represent the spatial and temporal variations of sulfur dioxide concentration within the gas phase and its exchange with the solid phase through the gas–solid interfacial area.

2.3. Mass Balance in the Continuous Phase

Equations (10) and (11) represent the mass balance within the continuous phase. In these equations, the reaction rate—denoted by r—is incorporated to account for the chemical conversion of sulfur dioxide. The reaction rate is determined using Equation (12), which follows first-order kinetics. It is important to note that the reaction rate is directly affected by the sulfur dioxide concentration within the continuous phase.

$$\dot{m}_{bcon.}\mid_z - \dot{m}_{bcon.}\mid_{z+\Delta z} - \dot{m}_{mcon.} - \dot{m}_r = m_{acc.} \tag{10}$$

$$AU_{mf}C_c\mid_z - AU_{mf}C_c\mid_{z+\Delta z} - NQ(C_c - C_d) - r = V_c\frac{\partial C_c}{\partial t} \tag{11}$$

The unreacted core model provides a suitable framework to describe this dependency. According to this model, the reaction initiates on the external surface of the catalyst particle and subsequently progresses through the remaining inner layers until the entire particle becomes deactivated. A schematic representation of the pilot-scale process is shown in Figure 3.
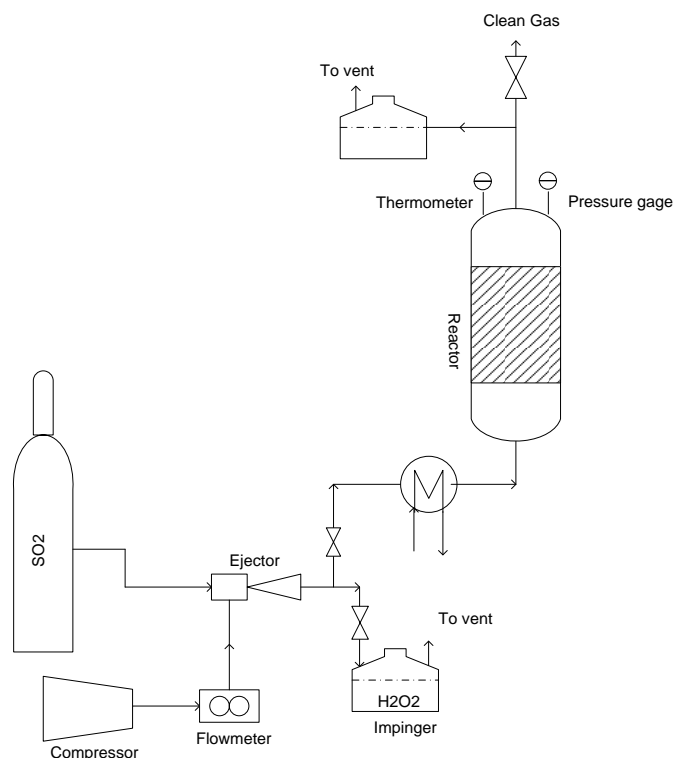
Fig. 3. Laboratory schematic of the pilot scale process.

To restore the catalytic activity, a regeneration process is required. Assuming that the catalyst particle size remains constant during the reaction, the overall reaction rate can be expressed by Equation (12). The global gas–solid reaction rate is governed by two primary diffusion resistances:

1. Intraparticle diffusion resistance, arising from mass transport through the porous layers of the catalyst, and

2. Chemical reaction resistance, associated with the intrinsic kinetics of the surface reaction.

The overall reaction rate constant, K, is defined by Equation (13), where Ks represents the intrinsic first-order rate constant, expressed by Equation (14).

$$r = kA_c C_c \tag{12}$$

$$k = \cfrac{1}{\cfrac{r_p(r_p - r_u)}{r_u D_{eff.}} + \cfrac{r_p^{\,2}}{r_u^{\,2} k_s}} \tag{13}$$

$$k_s = k_{so} \exp\left(\frac{-E_a}{RT}\right) \tag{14}$$

The pre-exponential factor in this relationship reflects the dependency of the reaction rate on the alumina content within the catalyst structure. The temporal variation of the unreacted-core radius within the catalyst particle is described by Equation (15).

$$\frac{1}{3r_p D_{eff.}} r_c^{\,3} - \frac{1}{2D_{eff.}} r_c^{\,2} - \frac{1}{k_s} r_c + \frac{1}{6D_{eff.}} r_p^{\,2} + \frac{1}{k_s} r_p - \frac{C_A}{\rho_p} t = 0 \tag{15}$$

Finally, the concentration of sulfur dioxide in each phase and in each reactor, compartment is obtained by simultaneously solving Equations (9) and (11), subject to the specified initial and boundary conditions, as defined in Equation (16).

$$C(t = 0) = C_0, C(z = 0) = C_{in} \tag{16}$$

3. Results and Discussion

An increase in the superficial gas velocity led to a corresponding enhancement in the efficiency of sulfur dioxide removal. This relationship is graphically illustrated in Figure 4. When the superficial gas velocity increased from 1.0 m/s to 1.8 m/s, the percentage of sulfur dioxide removed from the inlet gas rose from 50% to 90%. The increase in inlet flow rate directly translates into a higher gas velocity, which intensifies turbulence within the catalytic bed. This enhanced turbulence decreases the diffusional mass-transfer resistance between the

gas phase and the catalyst surface, thereby significantly improving the overall sulfur dioxide removal efficiency.
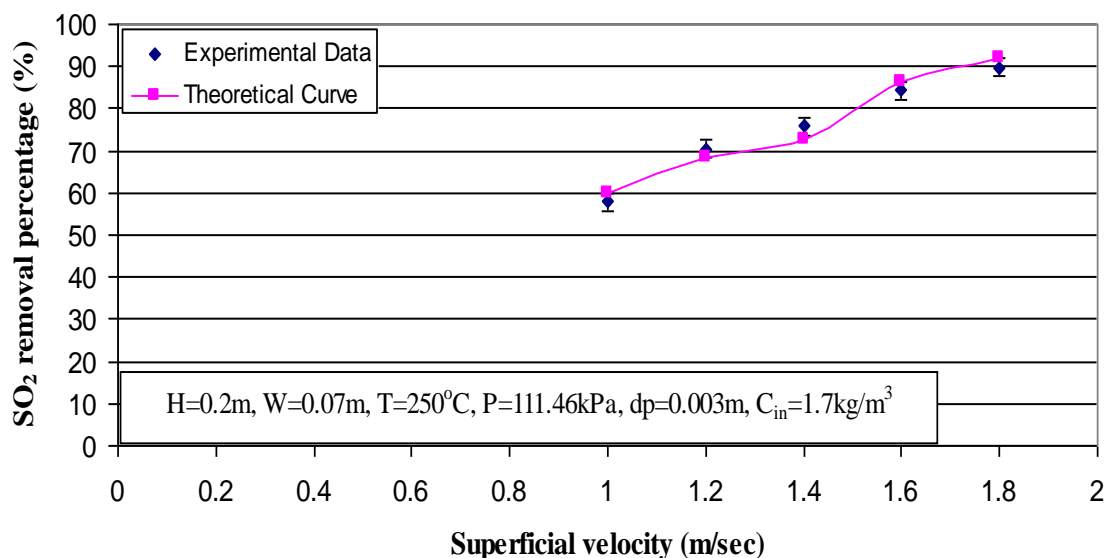

Fig. 4. Effect of superficial gas velocity on sulfur dioxide removal efficiency.

Figure 5 shows the effect of bed height on sulfur dioxide removal efficiency. The experimental results indicate that increasing the bed height by 0.15 m leads to a considerable improvement in SO_2 removal—from approximately 50% to 98%. This improvement can be attributed to the increase in the available mass-transfer surface area within the bed, which enhances process performance and, consequently, sulfur dioxide elimination. Increasing the bed height also extends the gas residence time within the reactor, facilitating more effective gas–solid contact. Furthermore, it was observed that increasing the bed height within the experimental range did not cause a significant pressure drop across the bed.

A series of experiments was conducted using three different bed widths: 7 m, 8 m, and 9 m. The corresponding sulfur dioxide removal efficiencies increased from approximately 57% to 63% and 69%, respectively. This enhancement can be explained by the larger reactor cross-sectional area, which provides a greater interfacial surface for mass transfer and, consequently, higher SO_2 removal rates. These results are graphically presented in Figure 5.
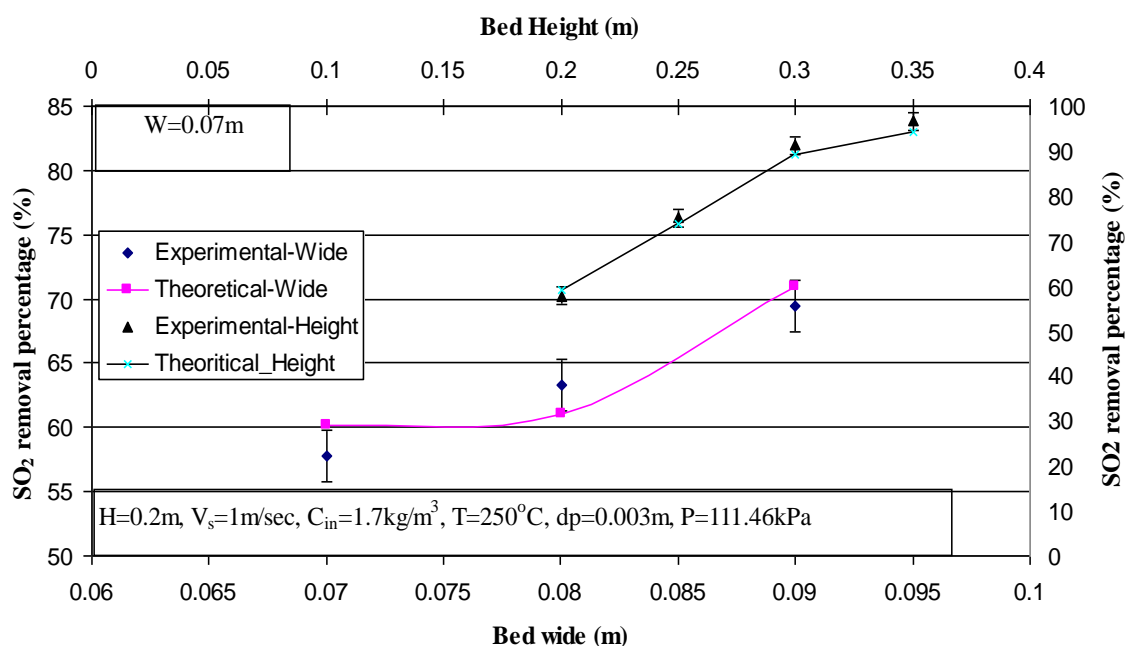
Fig. 5. Effect of bed height and width on sulfur dioxide removal efficiency.

Experimental data also revealed a positive correlation between the bed void fraction and the effective contact surface area, as illustrated in Figure 6. The bed void fraction refers to the portion of the reactor volume occupied by the catalyst particles, which directly affects gas–solid contact and diffusion rates.
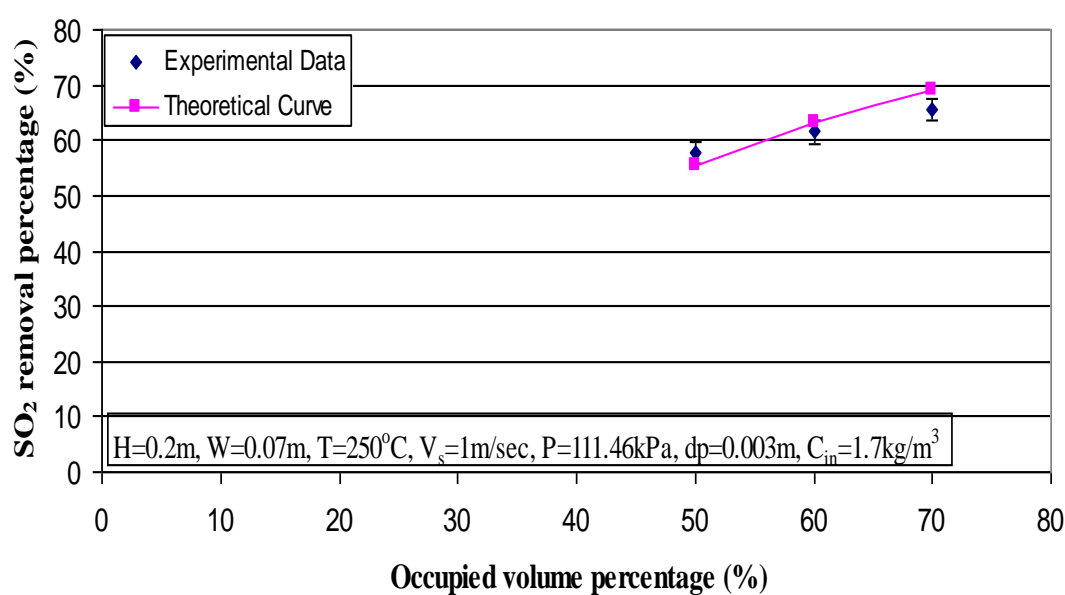

Fig. 6. Effect of bed occupied volume on sulfur dioxide removal efficiency.

Figure 7 demonstrates the positive influence of increasing the catalyst particle diameter on sulfur dioxide removal efficiency. Experiments were performed with catalyst particles of three distinct diameters: 2 mm, 3 mm, and 4 mm. Although an initial increase in particle size might appear to reduce the available external surface area for convective mass transfer, it simultaneously enhances the internal surface area available for diffusional mass transfer within the catalyst particles. As a result, an overall improvement in process performance was observed across this particle-size range. Figure 7 also illustrates the effect of the specific surface area of the bed on sulfur dioxide removal efficiency, confirming a positive correlation between catalyst surface area and the SO_2 adsorption rate within the bed.
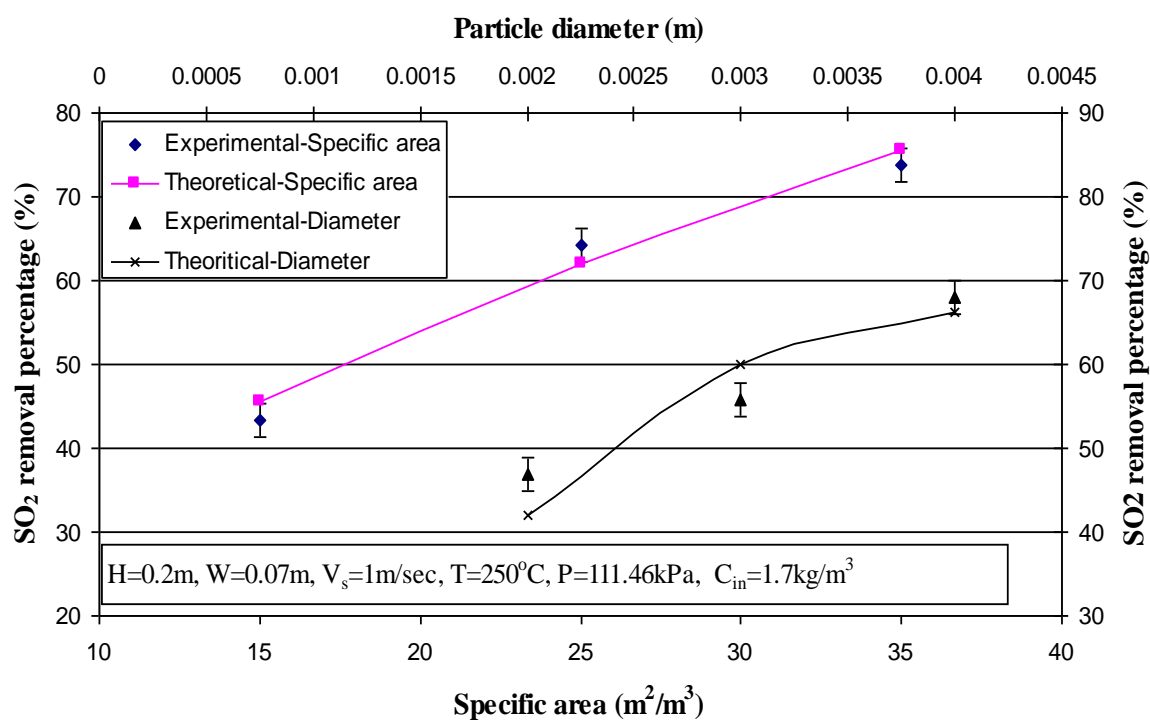

Fig.7. Effect of catalyst particle diameter and substrate specific surface area on sulfur dioxide removal efficiency.

Temperature is a key operational parameter that significantly affects the reaction kinetics and direction of catalytic processes. The impact of operating temperature was examined in this study. Higher temperatures increase the reaction rate between the catalyst and sulfur dioxide in the gas stream. As the operating temperature increased from 200 $^\circ$C to 450 $^\circ$C, the

SO_2 removal efficiency rose from approximately 52% to 97%. Moreover, the data presented in Figure 8 reveal a nearly linear relationship between operating temperature and the sulfur dioxide removal percentage within this temperature range.

As shown in Figure 8, an increase in operating pressure also led to a corresponding improvement in SO_2 removal efficiency. This effect can be attributed to the direct influence of pressure on the gas-phase mass-transfer coefficient, which facilitates enhanced diffusion of sulfur dioxide toward the catalyst surface.
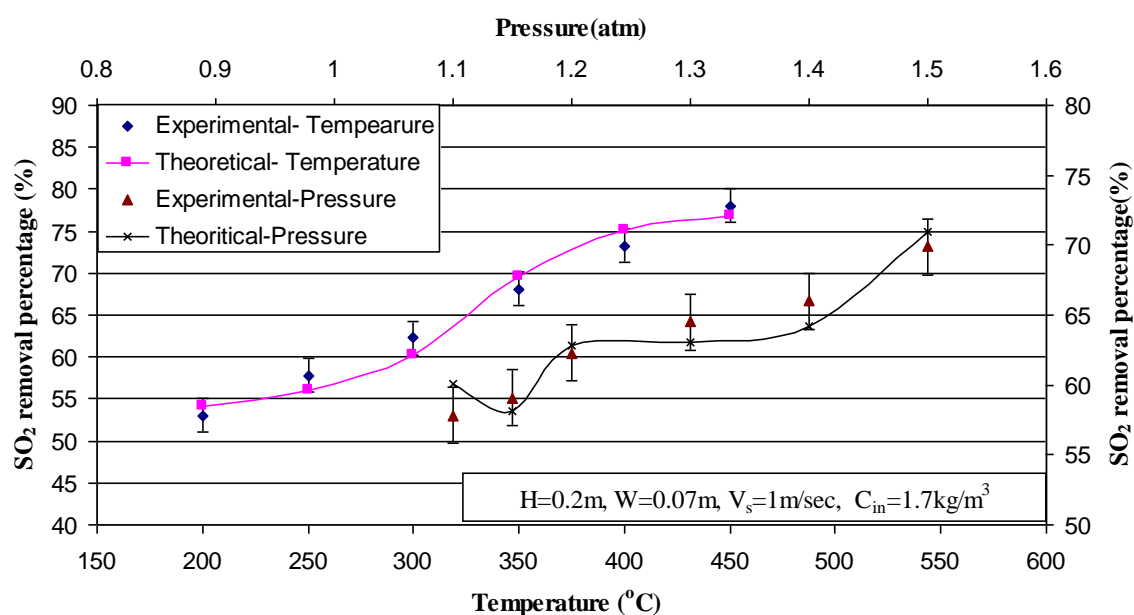

Fig.8. Effect of operating temperature and pressure on sulfur dioxide removal efficiency.

4. Conclusion

The results demonstrate that increasing the operating temperature, pressure, alumina adsorbent content, catalyst particle diameter, bed height, bed width, gas superficial velocity, and specific surface area all exhibit a positive correlation with sulfur dioxide removal efficiency.

In particular, an increase in bed height by only 0.15 m resulted in a remarkable 39% improvement in SO_2 removal efficiency, reaching a maximum value of approximately 99%.

Similarly, increasing the gas superficial velocity from 1.0 m/s to 1.8 m/s led to a substantial 30% improvement in removal efficiency—from 60% to 90%.

Furthermore, increasing the alumina content within the catalyst significantly enhanced sulfur dioxide removal performance. The optimum range for the alumina content was found to be between 12% and 15%, which minimizes catalyst attrition while maintaining high reactivity.

While increasing the operating pressure from 110 kPa to 150 kPa resulted in a moderate improvement in SO_2 removal efficiency—from 60% to 70%—this effect was less pronounced compared to other operating parameters.

The study confirms that all the aforementioned parameters influence the mass-transfer surface area, gas–solid contact time, or turbulence intensity within the fluidized bed reactor. In addition, both experimental and theoretical results verified the dependence of the mass-transfer coefficient on temperature and the reaction rate constant on the adsorbent content.

A comparison between the experimental data and the model predictions showed an average deviation of 2.7%, indicating strong agreement and validating the reliability of the developed mathematical model.

References

[1] Andoglu Coskun, E. M., Kaytakoglu, S., Manenti, F., & Di Pretoro, A. Using Reduced Kinetic Model for the Multi-Objective Optimization of Thermal Section of the Claus Process Leading to a More Cost-Effective and Environmentally Friendly Operation. *Processes*. 12(1) (2024)197.

[2] Ardeh, A. Z., Fathi, S., Ashtiani, F. Z., Fouladitajar, A. Kinetic modeling of a Claus reaction furnace and waste heat boiler: Effects of H_2S/CO_2 and H_2S/H_2O ratio on the production of hazardous gases in an industrial sulfur recovery unit. *Separation and Purification Technology*. 338(2024) 126173.

[3] Medhat, A., Shehata, W., Gad, F., Bhran, A. Process simulation, optimization, and cost analysis of a proposed sulfur recovery unit by applying modified Claus technology. *Journal of Engineering and Applied Science* .71(2024)109.

[4] Zahid, M. A., Ahsan, M., Ahmad, I., & Khan, M. N. A. Process Modeling, Optimization and Cost Analysis of a Sulfur Recovery Unit by Applying Pinch Analysis on the Claus Process in a Gas Processing Plant. *Mathematics*. 10(1) (2022) 88.

[5] An, S., Jung, J. C. Kinetic modeling of thermal reactor in Claus process using CHEMKIN-PRO software. *Case Studies in Thermal Engineering*.21 (2020) 100694.

[6] Sergienko, N., Lumbaque, E. C., Radjenovic, J. (Electro)catalytic oxidation of sulfide and recovery of elemental sulfur from sulfide-laden streams. *arXiv preprint arXiv*.2411(2024)15162.

[7] Ghahraloud, A. Perspectives in the Synergetic Photothermocatalysis of Hydrogen Sulfide Decomposition for Hydrogen Production: A Comprehensive Review. *Energy & Fuels*. (2024) 234-247 .

[8] Spatolisano, E., de Angelis, A. R., Pellegrini, L. A. Middle Scale Hydrogen Sulphide Conversion and Valorisation Technologies: A Review. ChemBioEng Reviews, 9(4) (2022). 370–392.

[9] Kannan, P., Raj, A., Ibrahim, S., Abumounshar, N. (2022). Process integration of sulfur combustion with Claus SRU for enhanced hydrogen production from acid gas. *International Journal of Hydrogen Energy*. 47(25) 12456–12468.

[10] Sajjadi, B. A techno-economic analysis of solar catalytic chemical looping biomass refinery for sustainable production of high purity hydrogen. *Energy Conversion and Management*. 243(2021)

[11] Rahman, R. K., Ibrahim, S., Raj, A. Multi-objective optimization of sulfur recovery units using a detailed reaction mechanism to reduce energy consumption and destruct feed contaminants. Computers & Chemical Engineering, 128 (2019) 21–34.

[12] Ibrahim, S., Rahman, R. K., Raj, A. Dual-stage acid gas combustion to increase sulfur recovery and decrease the number of catalytic units in sulfur recovery units. *Applied Thermal Engineering*. 156(2019) 576–586.